Examination of Material Flow in Thick Section Friction Stir Welding of Aluminum Using a Stop-Action Technique

K. J. Colligan and S. K. Chopra
Concurrent Technologies Corporation
Johnstown, PA
USA

Abstract

A stop-action technique was used in this study to arrest the tool motion and thereby preserve the material surrounding the welding tool as it was during welding of 25-mm thick aluminum-lithium 2195 plate. This technique allowed study of the interaction between the workpiece material and the welding tool pin in the keyhole. Such methods are inherently imperfect, since some degree of deceleration occurs, but insight into the dynamics of material flow can be gained. A frustum-shaped welding tool pin was used in this study, with threads and flats cut into the surface. This study illustrates the role of these features in producing plastic deformation, and four distinct plastic deformation mechanisms for this type of tool are proposed.

## Introduction

Historically, experimental metal-flow visualization studies of the friction stir welding (FSW) process have employed either stop action techniques [1-5] or tracer materials of various kinds [6-10], or a combination of these. These studies, all done in aluminum alloys, are useful as a guide for numerical modeling of the welding process, for tool design efforts, and for providing insight into the weld zone structure produced by different tool designs. The evolution of welding tool design requires that these studies be periodically repeated or that new methods be developed to explore the effect of new tools on material flow.

An example of the difference in stir zone structure that can be produced by two different welding tool designs is shown in Figure 1. The photomicrograph on the left in this figure was produced using a cylindrical, threaded pin with an essentially flat tip. It is notable that the stir zone profile is significantly larger than the pin profile. The photomicrograph on the right side of the figure shows the stir zone profile compared to the pin profile for a frustum-shaped pin with flats. In this case the stir zone shape is very close to the pin shape, except for the upper portion of the weld. The photomicrographs in Figure 1 were taken from welds in plates with different thickness, but the general shape of stir zones produced by the two tool types is independent of plate thickness. This implies that these different pin designs transport material differently, giving rise to the different stir zone profiles. The present work was undertaken to study material flow produced by the frustum shaped pin profile with flats.

The fundamental difficulty of studying material flow in friction stir welds lies in the fact that there is presently no practical method to directly observe material flow during a weld. Techniques must be devised to allow indirect study after the weld has been completed. Tracer studies are carried out by embedding different alloys that give etching contrast or small pieces of materials having a density contrast to the base metal. Sectioning or radiography of welds can then be performed to reveal aspects of material flow. This technique is especially useful for determining the distribution of material in the stir zone compared to where it started.

Stop-action techniques are useful for studying material flow because they allow study of the interaction of the welding tool with the workpiece material in the keyhole region. Previous studies [1,2,5] used a technique of rapid retraction of the welding tool at the end of a weld, essentially “unscrewing” the welding tool from the workpiece, leaving the surrounding weld metal undisturbed. However, new welding tool designs that employ the use of reentrant features [11] prohibit this technique, since the features would disturb the material surrounding the pin during the retraction process.

An alternate stop action approach employed by others [3,4] and in the present study involves engaging the “emergency stop” control on the welding machine during a weld. This quickly removes power from the axis and spindle drives and causes the welding machine to rapidly decelerate to a stop, leaving the welding tool pin embedded in the workpiece. The end of the weld can then be serially sectioned or cut using wire electrical discharge machining (EDM) to remove the pin remnants so that the internal features of the weld can be studied. This technique offers the opportunity to study the inside of the keyhole approximately as it was during the weld.

## Experiment Procedure

The technique used in this study involved ending friction stir welds by engaging the emergency stop control on the welding machine, relying on the torque exerted on the welding tool to cause the spindle to quickly coast to a stop. The stop action weld for this study was made in 25-mm thick aluminum-copper-lithium 2195 plate aged to slightly under peak aging condition. The welding tool geometry and weld parameters are summarized in Table 1. The welds were made bead-on-plate in load control with the welding tool axis normal to the workpiece surface. A photograph of a pin that is representative of the tool used is shown in Figure 2. The workpiece material was approximately 200-mm wide by 600-mm long and 25-mm thick. After the weld progressed several inches along the plate the emergency stop control was engaged and water was immediately poured onto the plate to cause the plate to cool quickly, thus preserving the metallurgical structure that was present during the weld.

After welding, the plate was cut to extract a 50-mm square section of material with the pin remnant at the center. The block was then sectioned as shown schematically in Figure 3 using a wire-EDM machine. Each cut consumed approximately 0.25mm of material. The pin remnants were then extracted from the sections. The positions of the three flats in the figure approximately reflect their positions in the sectioned samples. Each sample was then photographed on light and electron microscopes. The images from the electron microscope were digitally combined to form montages for subsequent study.

## Results

A light photomicrograph of section G-3 is shown in Figure 4. This photograph shows that the keyhole wall generally reflected the surface features of the pin, forming an inverse replica of the pin geometry, with notable exceptions. The direction of tool rotation shown in this figure is maintained in all of the figures in this paper, with the welding tool being rotated counter-clockwise when viewed from above. The keyhole walls are viewed from the perspective of the center of the pin.

Montages of SEM images from samples G-1, G-2, and G3 are shown in Figures 5, 6 and 7, respectively. Higher magnification photomicrographs from sample G-3 are shown in Figures 8 and 9. Inspection of the right-hand portions of Figures 5 through 7 reveals workpiece material that was formed by the pin threads flowing into the spaces provided by the pin flats. Voids between the thread-formed material are observed in the area of the leading edge of each pin flat, as indicated in Figure 5. The voids were observed over most of the length of the pin, but generally were absent in the upper portion of the keyhole in this and other welds studied. The voids were much longer in the case of specimen G-3. The mid-section of each sample had material that was formed by the corresponding pin flat. Along the left side of each sample, material formed by the next threaded portion of the pin can be observed.

Higher magnification photomicrograph montages taken from specimen G-3 are shown in Figures 8 and 9. Figure 8 shows the region of extended flow of thread-formed workpiece material into the space created by the reentrant flat cut into the surface of the pin. The left end of the thread-formed material is concealed by a thin layer of aluminum in this portion of the keyhole. Figure 9 shows the thread-formed material from further down in specimen G3. Here the thread-formed material can be seen as it is compressed in the flat space, resulting in consolidation of the thread-formed material with the material carried in the flat. Along the trailing edge of the flat the thread-formed material from the next threaded portion of the pin can be seen as a replica of the pin geometry.

## Discussion

An analysis of the validity of the stop-action technique must include consideration of the deceleration process that took place as the spindle rotation and tool travel stopped. The deceleration time can be calculated by dividing the angular momentum of the rotating components by the spindle torque, taking care to account for any multiplication of the momentum provided by gears or pulleys. The angular momentum and spindle torque data for the weld presented here are summarized in Table 2. This calculation resulted in a predicted deceleration time of 0.15 seconds, or 0.27 revolutions based on an initial speed of 215 revolutions per minute. During deceleration the welding tool was still being pushed forward, even though the travel axis had its power quickly removed after engaging the emergency stop control. This forward force came from accumulated elastic strain energy stored in the welding machine's structure, since the machine is very large. Based on static load/deflection testing done on the machine, it is estimated that about 1.5 mm of elastic deflection was present during the weld, which is much greater than the 0.13 mm the tool would have traveled during the deceleration time, assuming linear deceleration.

Without high-speed data collection and specialized sensors it is impossible to measure the details of the deceleration process. However, it is possible to speculate on the deceleration process by examining the features in the keyhole produced. If the spindle rotation and axis travel decelerated to a stop precisely in unison, then the travel per revolution would not change during the deceleration period, and the keyhole produced would be representative of conditions present during normal welding. If the travel axis stopped while the spindle was still rotating one would expect the voids in one flat to be the same as in the others. In addition, the drop in travel distance per revolution would presumably produce voids over the length of the pin, not just in the lower portion of the pin. This is not what was observed in this study, since the voids in specimen G-3 were clearly larger than the voids in the other flats. Alternatively, if the travel deceleration started after the spindle began decelerating, which is reasonable since the decay in travel speed was in response to the decay in spindle speed, then one would expect higher than normal travel per revolution as the pin stopped. This would mean that the material captured within the flats was more than one would expect during normal welding. This conclusion is supported by inspection of the pin shown in Figure 2. The abrasion on the trailing edge of the flat on this pin is much narrower than the width of material in contact with the flats observed in this study, suggesting that the conditions present as the pin decelerated represented a higher travel per revolution that would normally be expected. In spite of this distortion, general conclusions about the material flow can be developed.

A pin that has no flats produces a stir zone that is much wider than one that has flats, as illustrated in Figure 1. It is apparent from inspection of the stop-action welds produced in this study that the flats provide a key mechanism for transporting material around the pin from within the pin profile. By providing a new path for material transport, this mechanism obviates the need for material to extrude around the retreating side of the pin, thereby reducing the width of the stir zone. Each flat instead captures the material in the path of the pin as it rotates in front of the pin and deposits material as it rotates behind the pin.

A number of observations can be made about material flow during welding by inspection of Figures 4 through 9, keeping in mind that the travel distance per revolution at the instant of stopping the spindle was probably higher than that in normal welding conditions. In this weld it is clear that the threads were generally full of workpiece material during welding, since the keyhole wall precisely reflected the geometry of the space between the pin's threads, or thread spaces. The flat spaces were generally full of workpiece material as well, except for the voids that were observed along the leading edge of the flats, especially prominent in specimen G-3 in Figure 7.

The voids in the flat spaces suggest that during welding workpiece material within the thread spaces extruded into the flat space, but retained the shape of threads for a time. This was especially evident in specimen G-3. As the tool continued to rotate, this thread-shaped material was deformed as it contacted the material carried within the flat space. The workpiece material then extruded into the thread spaces on the trailing edge of the flat and presumably continued down with the general motion of the threads. This indicates that the flat is responsible for producing plastic work as the thread-shaped material contacts the material carried within the flat space is deformed and combined, and is extruded into the next thread space segment. The typically small thermo-mechanically affected zone, as shown in Figure 1, suggests that the above deforming-combining-extruding events occur within the flat space. In addition, if the material within the flat space rotates with the pin, then there would be shear deformation between this material and the surrounding workpiece material, which is presumably not rotating.

The appearance of thread-formed material in the flat space implies that there is relative sliding between the pin threads and the material in the thread spaces. If this is the case, the helical shape of the threads then requires that the material within the threads is driven downward with the apparent downward motion of the threads as the tool rotates. This would necessarily produce downward plastic shear of material along the surface defined by the crowns of the pin threads. The shear would presumably take place at a rate defined by the thread pitch and the relative rotation speed.

The plastic work produced by the welding tool pin is illustrated in Figure 10. In this drawing the curved surface of the pin is flattened out to a plane as an aid for visualization. The drawing shows a section of the welding tool and workpiece. Since the tool has been "unwound", the flat appears as a curved surface in this drawing. As can be seen in the figure, the workpiece material in the thread spaces exactly conforms to the shape of the pin, but as this material enters the flat space it retains its shape until it is squeezed into material carried within the flat. This material then extrudes into the next set of thread spaces on the trailing edge of the flat.

Based on these observations, the pin may be responsible for at least three and possibly four distinct plastic deformation processes, as shown in Figure 10. First, material within the thread space appears to slide with respect to the pin, which requires that the material is simultaneously being pushed downward by the threads and sheared along a surface defined by the thread crowns (note A in Figure 10). Second, thread-formed material is plastically deformed as it contacts the material carried within each flat, combines with this material, and is extruded into the next set of threads (note B). A third deformation process occurs in the form of shear between material carried within the flat spaces and material outside of the pin (note C). The downward shear produced by the threads occurs at a velocity that is a function of the thread pitch and the rotational speed, while the plastic work within the flats and between the material within the flats and the material outside of the pin occurs at a speed that is proportional to the peripheral velocity of the pin.

A fourth plastic deformation process is possible with this tool design, although it was not directly observed in this study. It is presumed that the trailing edge of each flat captures material due to the forward travel of the tool as the flat rotates around the front of the pin. It is speculated that this process would only take place along the leading edge of the pin, where the forward advance of the tool causes a forward component to the motion of the trailing edge of the flats in addition to the circumferential component produced by pure rotation. On the trailing side of the pin, one would expect the flats to be responsible for expelling material into the stir zone by the opposite process. This implies that the flats act as a means for collecting, transporting, and expelling material behind the pin. This speculation is supported by the observation that in the welds done in this study a variation in the amount of material carried in the flats was observed, with flats that were on the advancing side of the pin being less full than those on the retreating side were. This can be seen by comparing sample G-3 in Figure 7 with the other two sections.

## Conclusions

In this study a method of performing a stop-action friction stir weld in thick section 2195 Al-Li was used, followed by sectioning of the keyhole and removal of the pin remnants, to observe the workpiece/pin interaction. A frustum-shaped, threaded pin with flats was used. The keyhole wall was generally an inverse replica of the pin geometry, with notable exceptions. Based on study of the keyhole, four modes of pin-induced plastic work are proposed. These plastic work modes include downward shear of material within the pin threads relative to the surrounding material, compression of thread-formed material in the flats, circumferential shear at the peripheral velocity of the pin occurring within the flats, and capture of material by the trailing edge of the flats as they rotate around the front of the pin.

## References


1. Colligan, K.J., "Dynamic Material Deformation During Friction Stir Welding In Aluminum," *Proc. 1st Int. Sym. on Friction Stir Welding*, Thousand Oaks, USA 1999.
2. Colligan, K.J., "Material Flow Behavior During Friction Stir Welding," *Welding Journal*, July 1999.
3. Guerra, M., McClure, J.C., Murr, L.E., and Nunes, A.C., "Metal Flow During Friction Stir Welding," *Friction Stir Welding and Processing*, TMS, 2001.
4. McClure, J.C., Coronado, E., Aloor, S., Nowak, B.M., Murr, L.E., and Nunes, Jr., A.C., "Effect of Pin Tool Shape on Metal Flow During Friction Stir Welding," *Proc. 6th Int. Conf. on Trends in Welding Research*, April 15-19, 2002, Pine Mountain, GA, USA.
5. Dickerson, T., Shercliff, H.R., and Schmidt, H., "A Weld Marker Technique for Flow Visualization in Friction Stir Welding," *Proc. 4rth Int. Sym. on Friction Stir Welding*, Park City, Utah, 2003.

6. Reynolds A.P., Seidel, T.U., and Simonsen, M., "Visualization of Material Flow in an Autogenous Friction Stir Weld," *Proc. 1st Int. Sym. on Friction Stir Welding*, Thousand Oaks, USA 1999.
7. Seidel, T.U. and Reynolds, A.P., "Visualization of the Material Flow in AA2195 Friction Stir Welds Using a Marker Insert Technique," *Metallurgical and Materials Transactions A*, 32A, 2001.
8. London, B., Mahoney, M., Bingle, W., Calabrese, M., and Waldron, D., "Experimental Methods for Determining Material Flow in Friction Stir Welds," *," Proc. 3rd Int. Sym. on Friction Stir Welding,* Kobe, Japan, 2001.
9. Ouyang, J.H., Kovacevic, R., Jandric, D., Song, M., and Valant, M., "Visualization of Material Flow During Friction Stir Welding of the Same and Dissimilar Aluminum Alloys," *Proc. 6th Int. Conf. on Trends in Welding Research*, April 15-19, 2002, Pine Mountain, GA, USA.
10. London, B., Mahoney, M., Bingel, W., Calabrese, M., Bossi, R.H., and Waldron, D., "Material Flow in Friction Stir Welding Monitored with Al-SiC and Al-W Composite Markers," *Friction Stir Welding and Processing II*, TMS, 2003.
11. Thomas, W.M., Nicholas, E.D., Needham, J.C., Temple-Smith, P., Kallee, S.W.C.W, and Dawes, C.J., "Friction Stir Welding," *UK Patent Application*, May 7, 1997.

Acknowledgements

This work was sponsored by the Tank-Automotive Research Development & Engineering Center and prepared by the National Center for Excellence in Metalworking Technology, operated by Concurrent Technologies Corporation (CTC), under Contract No. N00014-00-C-0544 to the Office of Naval Research as part of the Navy ManTech Program. Approved for public release; distribution is unlimited. The photomicrograph on the left side of Figure 1 was used by permission of Lockheed Martin.

Table 1. Welding tool geometry and weld parameters.

| | |
|---|---|
| Shoulder Profile | flat shoulder with scrolls |
| Shoulder Diameter, mm | 30.5 |
| Shoulder Material | H13 |
| Pin Profile | threaded frustum with flats |
| Pin Root/Tip Diameters, mm | 15.2/8.9 |
| Pin Length, mm | 24.6 |
| Pin Material | MP159 |
| Number of Flats | 3 |
| Spindle Speed, rev/min | 220 |
| Travel Speed, mm/min | 102 |

Table 2. Estimate of rotation during spindle deceleration.

| Item | Mass Moment of Inertia, kg-m^2 | Pulley Ratio | Mass Moment About Spindle, kg-m^2 | Force Moment, N-m-s^2 | Angular Momentum, N-m-s |
|---|---|---|---|---|---|
| Spindle Shaft | 0.23 | 1 | 0.23 | 0.23 | 5.13 |
| 60-Taper Tool Holder | 0.02 | 1 | 0.02 | 0.02 | 0.45 |
| Tool Holder Collar | 0.05 | 1 | 0.05 | 0.05 | 1.06 |
| Spindle End Cap | 0.10 | 1 | 0.10 | 0.10 | 2.22 |
| Thrust Washer | 0.01 | 1 | 0.01 | 0.01 | 0.13 |
| Bearing Locknut | 0.01 | 1 | 0.01 | 0.01 | 0.12 |
| Inner Race Spacer | 0.04 | 1 | 0.04 | 0.04 | 0.81 |
| Drive Sprocket | 0.33 | 1 | 0.33 | 0.33 | 7.48 |
| Motor Sprocket | 0.01 | 2.76 | 0.02 | 0.02 | 0.42 |
| Drive Sprocket Bushing | 0.01 | 1 | 0.01 | 0.01 | 0.12 |
| Motor Sprocket Bushing | 0.00 | 2.76 | 0.00 | 0.00 | 0.07 |
| Spindle Drive Motor | 0.57 | 2.76 | 1.58 | 1.58 | 35.58 |
| Rotational Speed (rad/sec) | 22.51 | Total Angular Momentum, N-m-s | | | 53.59 |
| Torque (N-m) | 360.6 | Deceleration time, s | | | 0.15 |
| | | Angular Rotation, rev | | | 0.27 |

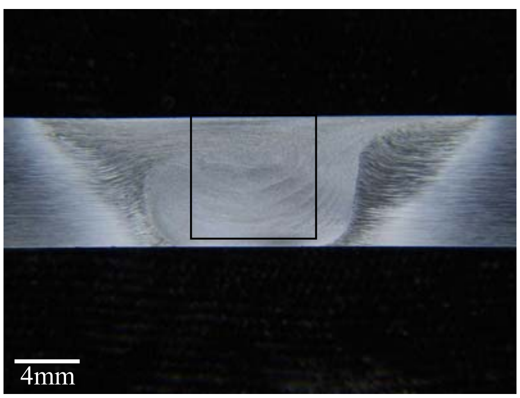

8.1-mm thick 2195 weld cross section

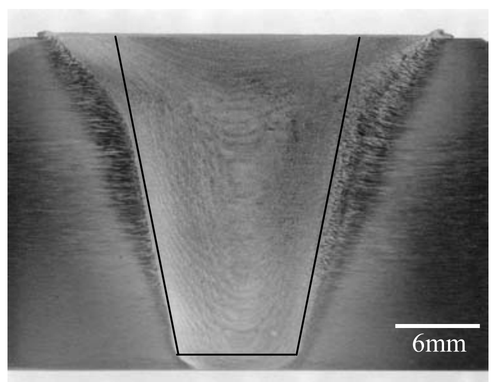

25.4-mm thick 2195 weld cross section

Figure 1. Representative weld cross sections produced by two different welding tool designs – l) produced by a cylindrical threaded pin (approximate profile shown), r) produced by a frustum-shaped threaded pin with three flats.

Figure 2. MP159 pin, representative of the pin used this study.

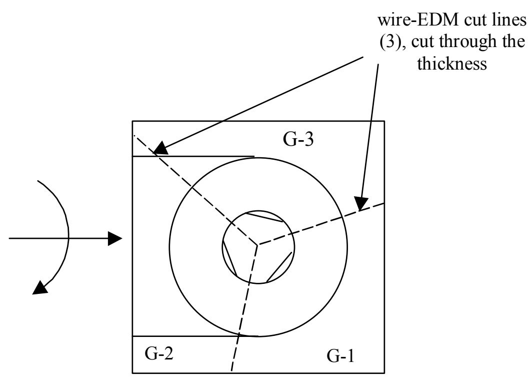


Figure 3. Cutting sketch for removing the pin remnants.

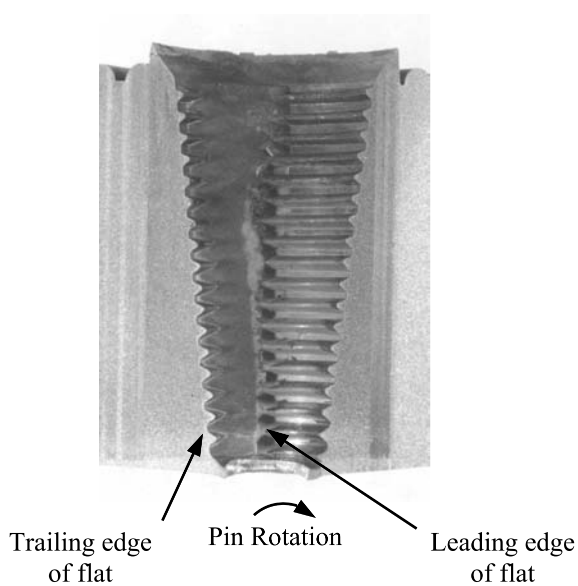


Figure 4. Optical photomicrograph of keyhole wall from section G-3.

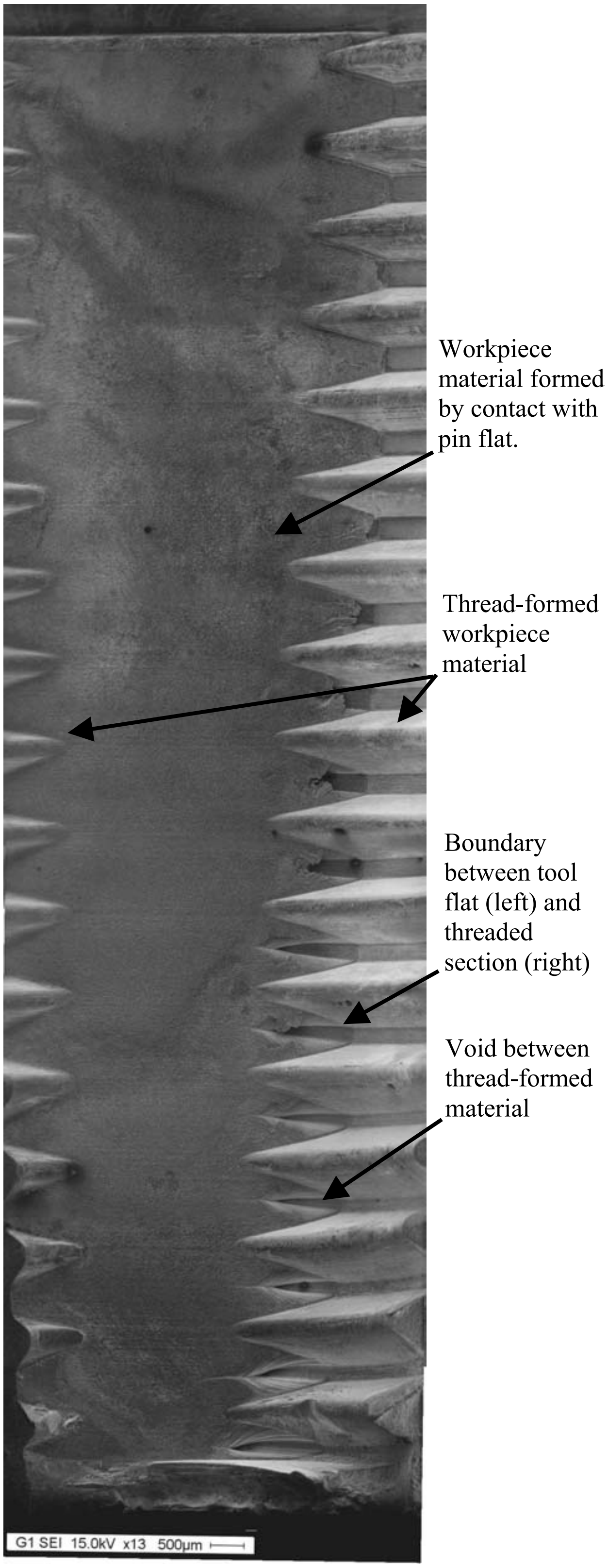


Figure 5. Digital montage of SEM images taken from section G-1.

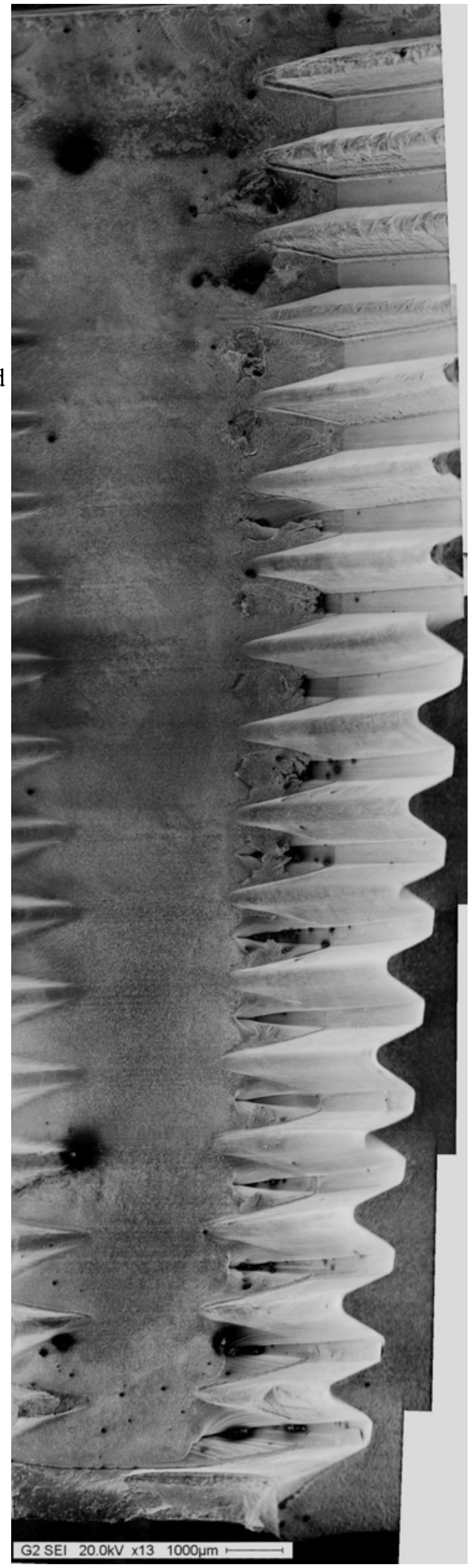


Figure 6. Digital montage of SEM images taken from section G-2.

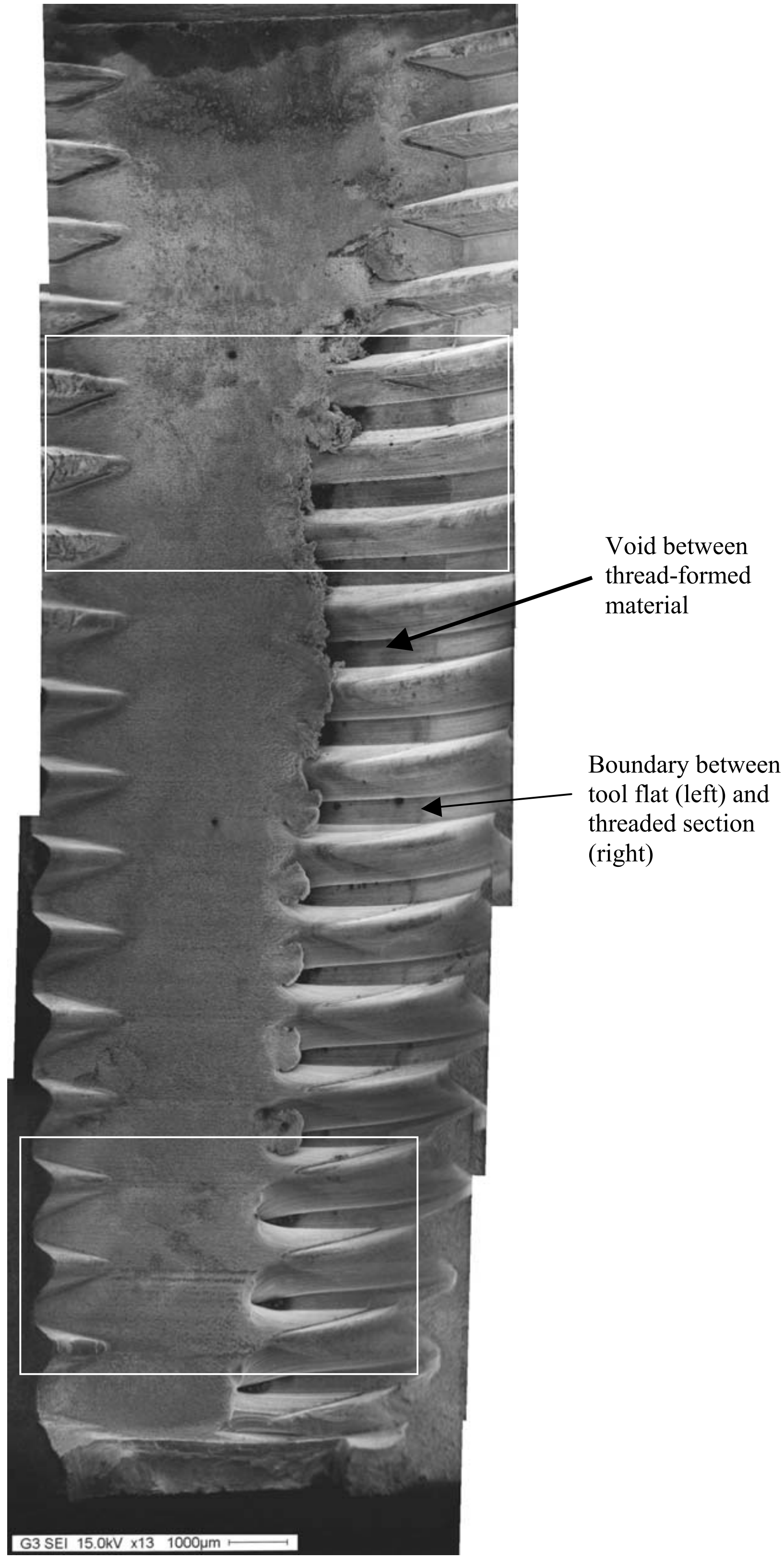


Figure 7. Digital montage of SEM images taken from section G-3 (boxes indicate boundary of higher magnification photomicrographs in Figure 7 (top) and 8 (bottom)).

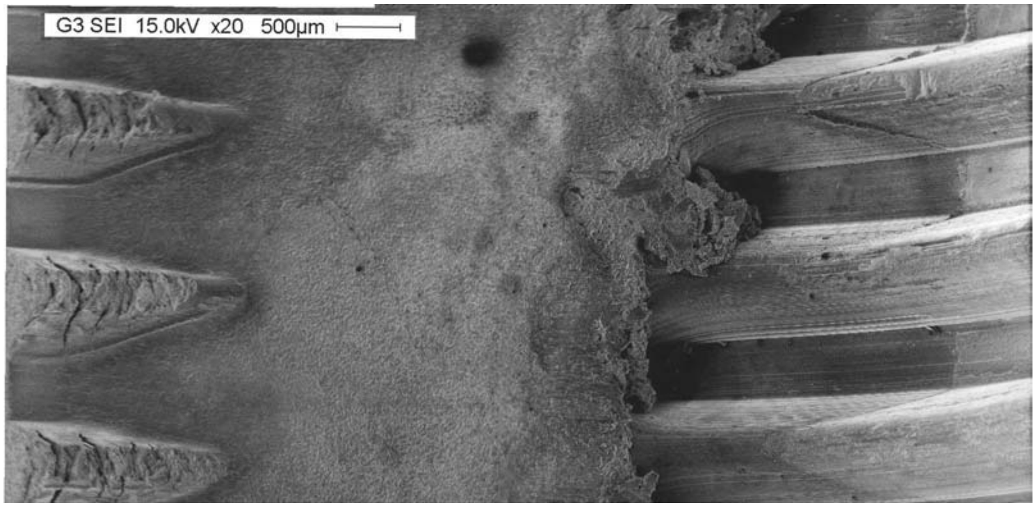


Figure 8. Representative SEM photomicrograph from section G-3.

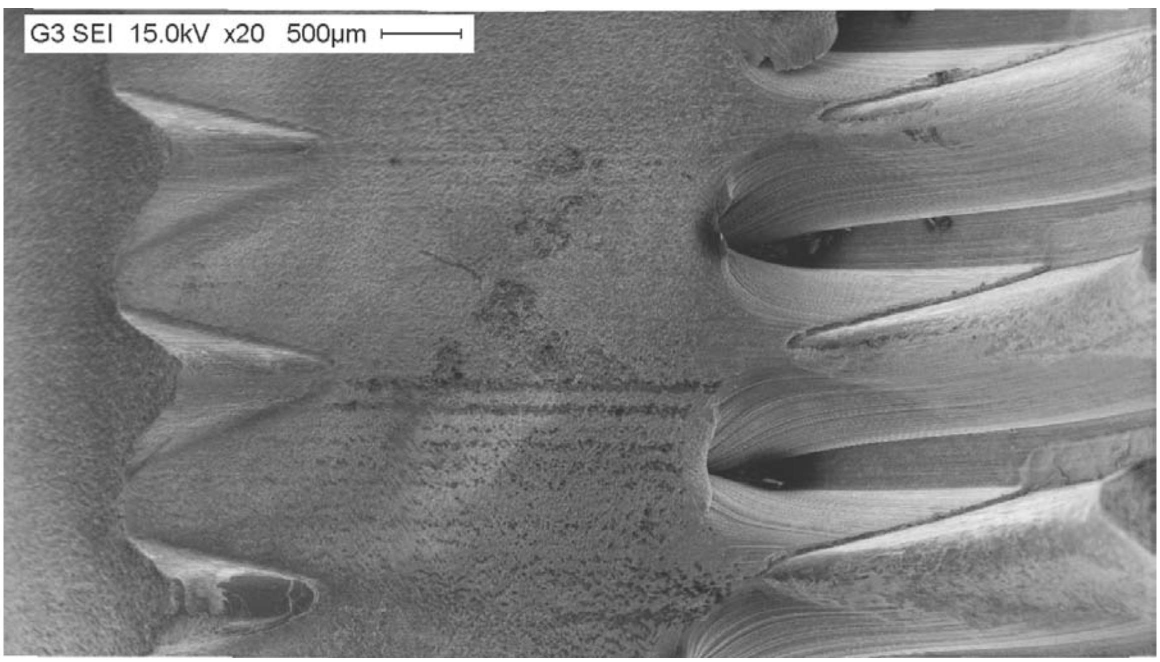


Figure 9. SEM image from section G-3, voids in leading edge of flat, arrows indicate edge of region of contact with flat.

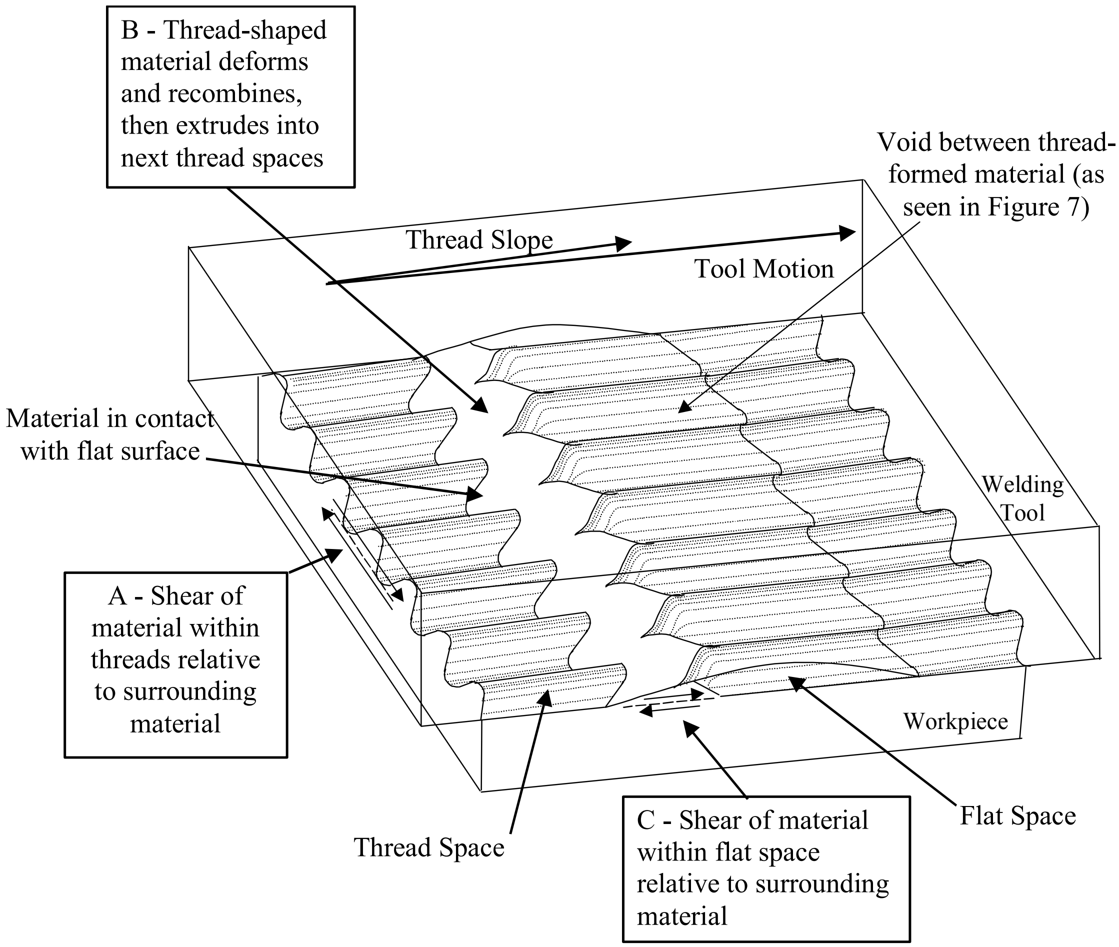


Figure 10. Illustration of material flow in the flat space.